

A Model-free Approach for Profiling of Polydisperse Soft Matter Using Small Angle Scattering

Guan-Rong Huang,^{*,†} Chi-Huan Tung,[‡] Lionel Porcar,[¶] Yangyang Wang,[§] Yuya
Shinohara,^{||} Changwoo Do,[⊥] and Wei-Ren Chen^{*,⊥}

[†]*Department of Materials and Optoelectronic Science, National Sun Yat-sen University,
Kaohsiung 80424, Taiwan*

[‡]*Department of Materials Science and Engineering, National Tsing Hua University,
Hsinchu 300044, Taiwan*

[¶]*Institut Laue-Langevin, B.P. 156, F-38042 Grenoble cedex 9, France*

[§]*Center for Nanophase Materials Sciences, Oak Ridge National Laboratory, Oak Ridge,
Tennessee 37831, United States*

^{||}*Materials Science and Technology Division, Oak Ridge National Laboratory, Oak Ridge,
Tennessee 37831, United States*

[⊥]*Neutron Scattering Division, Oak Ridge National Laboratory, Oak Ridge, Tennessee
37831, United States*

E-mail: huangrn@mail.nsysu.edu.tw; chenw@ornl.gov

Abstract

A strategy for determining the size polydispersity of systems from their small angle coherent scattering is outlined. Using the method of moment expansion, we show that the various central moments representing the average particle size, variance of

particle size, and skewness of size distribution function (SDF) for polydisperse systems can be unbiasedly extracted from spectral analysis. When the degree of polydispersity is moderate, SDF can be further reconstructed based on the maximum entropy principle. Numerical benchmarking of a model study over a wide range of size nonuniformity demonstrates the validity of this analytical approach for quantifying the size distribution of general soft matter systems in a model-free manner.

Introduction

Many soft materials, including colloids, polymers, micelles, microemulsions, and vesicles, exhibit a continuous size distribution of constituent particles. The profound influence of this polydispersity on the thermodynamic properties of practical materials, which are not encountered in the ideal monodispersed counterparts, has been long recognized¹. Much interest has been in establishing a unifying description of polydisperse soft matter's equilibrium phase and transport behaviors to provide insight into the de novo design of new multicomponent systems with customized properties^{2,3}. Since this continuous endeavor of theory and computation demands as its starting point the degree of non-uniformity in size, the experimental determination of its polydispersity naturally becomes of paramount interest.

Prominent among the available tools for characterizing polydispersity in soft matter is small angle scattering (SAS). Using SAS, the size distribution function (SDF) can be obtained from scattering spectra measured in the reciprocal space. The SDF is commonly treated as a weight function associated with the form factor of the particle in the numerical integration for regression analysis. The prerequisite of this existing protocol is to identify an explicit parametric expression of SDF^{4,5}. However, it has been long recognized that the validity of selected SDF for many systems, such as the self-organizing structures of novel multicomponent materials, often cannot be determined in advance⁶⁻⁹.

To circumvent the deficiency inherent to the current protocol, we propose a fundamentally new framework for determining the SDF of general soft matter systems from their

scattering signature: Its mathematical essence is that the parametric expression of SDF is no longer required as an input in regression analysis. Instead, by decomposing SDF using the moment expansion scheme, relevant moments representing the mean, variance, skewness, and kurtosis of size polydispersity are extracted in a model-free manner from the measured coherent scattering. Based on the principle of maximum entropy, the SDF is accordingly reconstructed, and its quantitative accuracy is confirmed through numerical benchmarking.

Central Moment Expansion Method

We outline the mathematical details of our proposed inversion framework, central moment expansion (CME) method, using non-interacting systems consisting of hard and soft globular particles with different sizes as a demonstration of its effectiveness.

Size Polydispersity Effect in Scattering Intensity

To describe the size distribution function (SDF) of a polydisperse system, we can express it as an unknown function $f(R)$ that is dependent on the size of the constituent particles R . Since the sum of all its possible results must be equal to one, it is required that $\int_0^\infty dRf(R) = 1$. Accordingly, the mean and variance of particle size can be represented as $\bar{R} \equiv \int_0^\infty dRf(R)R$ and $\sigma_R^2 = \overline{R^2} - \bar{R}^2 \equiv \int_0^\infty dRf(R)(R - \bar{R})^2$, respectively. The coherent scattering cross section $I(Q)$ can be expressed as

$$I(Q) = n\Delta\rho^2 \int_0^\infty dRf(R)G(Q, R), \quad (1)$$

where n is the particle number density, $G(Q, R) \equiv v^2(R)P(QR)$, $P(QR)$ is the normalized particle form factor, $v(R)$ is the volume of a molecular aggregate as a function of R . For a spherical particle, $v(R) = \frac{4}{3}\pi R^3$. Equation (1) reduces to the familiar expression for non-interacting monodisperse systems. In this limit, $f(R)$ is a Dirac delta function centered at $R = \bar{R}$, and $I(Q) = n\Delta\rho^2 f(\bar{R})G(Q, \bar{R})$. Two commonly encountered SDFs, the asymmetric

Schulz and symmetric beta distributions of two non-interacting systems consisting of spherical particles are given in Fig. 1. Here the parameter of polydispersity index $p \equiv \sigma_R/R$ is used to quantify the nonuniformity in particle size. Upon increasing p the widths and heights of both SDFs are seen to be steadily broadened and shortened as indicated by panels (a) and (c) in Fig. 1. The skewness of Schulz distribution given in panel (a) becomes visually discernible when $p > 0.15$. Two characteristic developments of $I(Q)$ are triggered by the increasing size heterogeneity, as displayed in Fig. 1 (b) and (d): Firstly, the intensity of $I(Q)$ in the region of $Q\bar{R} < 2$ is seen to progressively enhance with an increase in p . Secondly, as indicated by the insets in the log-linear scale, the oscillating minimum at $Q\bar{R} = 4.5$ is smeared simultaneously. Moreover, the comparison of $I(Q)$ for Schulz system given in Fig. 1(b) and that for Beta system given in Fig. 1(d) clearly shows that the skewness of SDF renders an additional increase in the coherent scattering intensity. As shall be demonstrated later in Fig. 2(a), the enhancement becomes more significant when p is larger.

To advance understanding of the connection between the characteristic variation of $I(Q)$ and SDF, we explore the behavior of Eqn. (1) as Q approaches zero. Since $P(0) = 1$ in this limit,

$$\lim_{Q \rightarrow 0} I(Q) \equiv I(0) = n\Delta\rho^2 \int_0^\infty dR f(R) v^2(R) \propto \bar{v}^2. \quad (2)$$

Equation (2) suggests that the forward coherent scattering, which can be obtained by extrapolation experimentally, is determined by the average of the square of particle volume \bar{v}^2 , as expected from the Rayleigh scattering law. One common measure of the size fluctuation in a polydisperse system is the ratio between \bar{v}^2 and the square of average of particle volume \bar{v}^2 . One can infer from the comparison of Fig. 2(a) and Fig. 2(b) that the mean-field value of $I(0)$ is a collective reflection of several central moments of SDF including the first one representing \bar{R} , the second one representing σ_R^2 , the third one representing the skewness β_1 , and the fourth one representing the kurtosis β_2 .

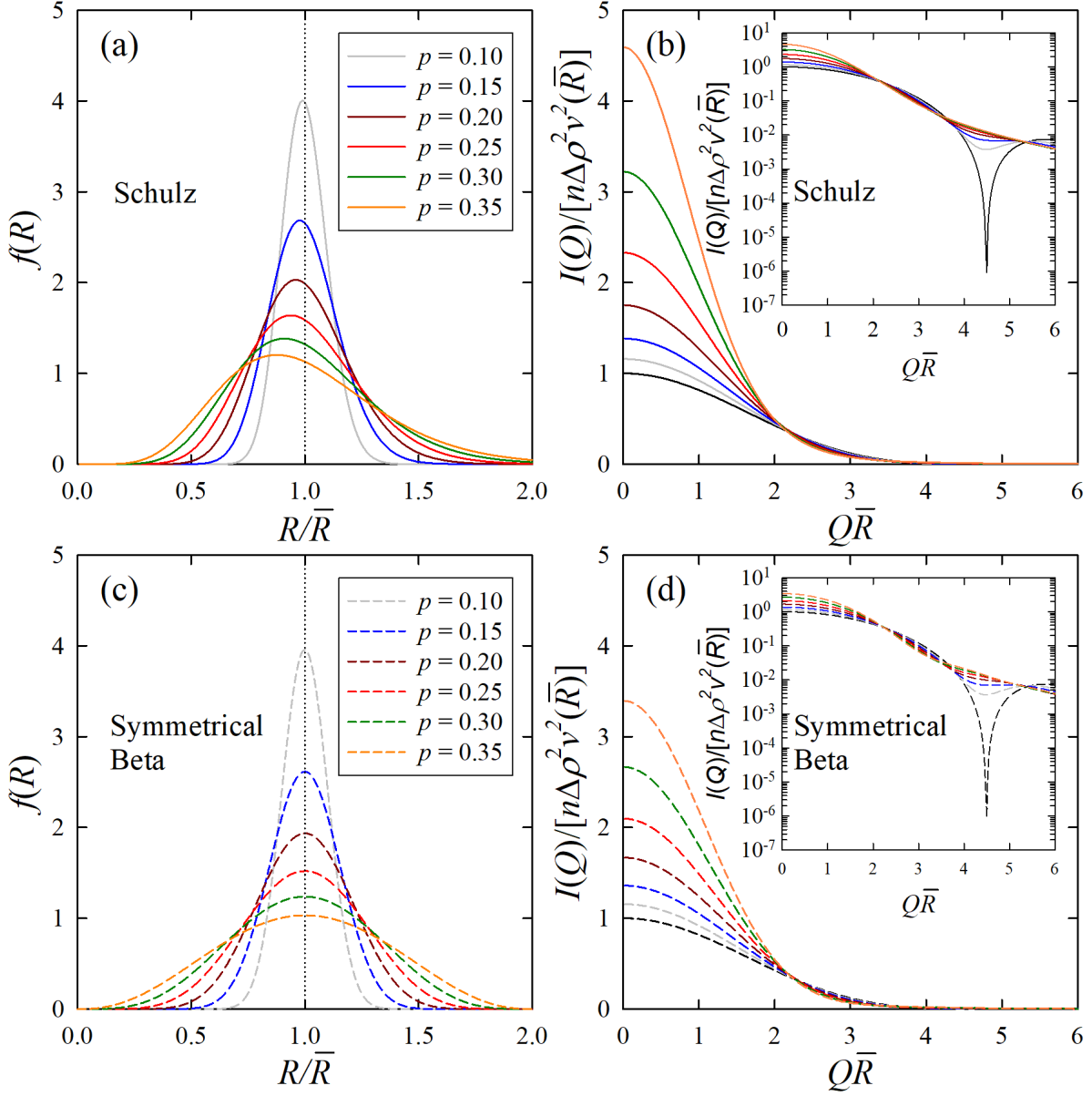


Figure 1: Continuous Schulz distribution (a) and symmetrical beta distribution (c) of hard-sphere diameters for six different degrees of polydispersity, where monodisperse form factor $P(x) = 9(\sin x - x \cos x)^2/x^6$. The x -axis of both distributions is normalized by the mean particle size \bar{R} . The dotted lines are used to facilitate the visual inspection of skewness. The associated coherent scattering cross section $I(Q)$ in the linear scale are given in panels (b) and (d) respectively. The y -axis of $I(Q)$ is normalized by $n\Delta\rho^2v^2(\bar{R})$. The corresponding log-linear plots are given in the insets.

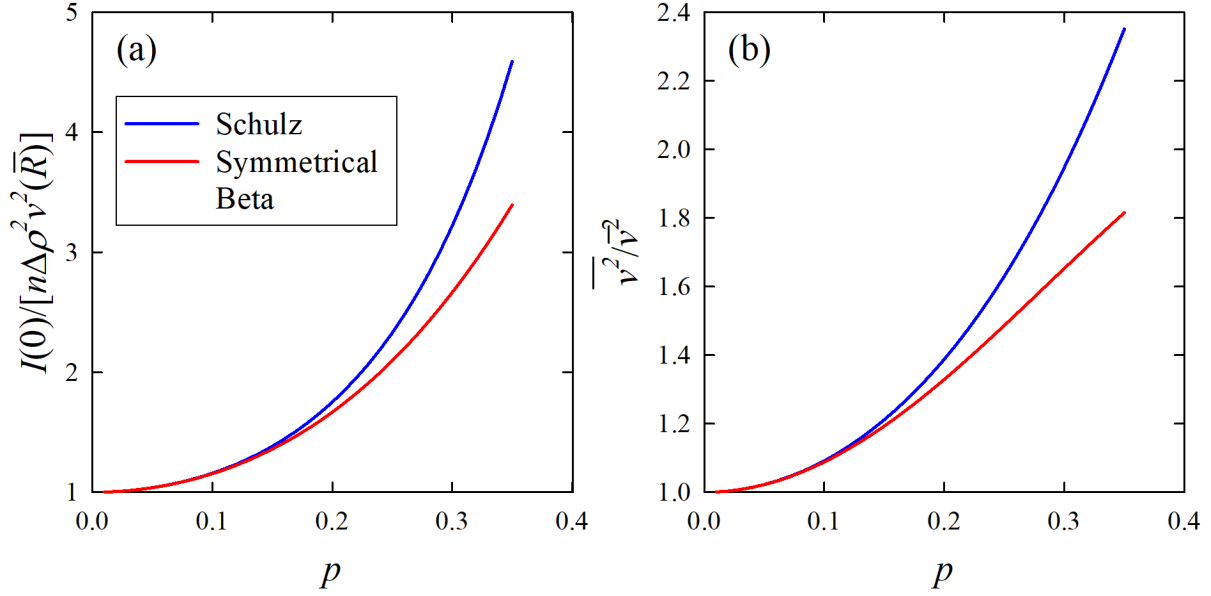


Figure 2: (a) The corresponding forward coherent scattering as a function of polydispersity index p for non-interacting systems consisting of hard sphere particles with polydispersity modeled respectively by Schulz distribution (blue curve) and symmetrical Beta distribution (red curve). (b) The corresponding fluctuation of particle volume.

Central Moment Expansion

To determine the central moments related to \bar{R} , σ_R^2 , β_1 , and β_2 of the SDF, the analysis of $I(Q)$ in the intermediate Q regime is required. To this end, one can further expand Eqn. (1) with respect to R as

$$I(Q) = n\Delta\rho^2 \int_0^\infty dR f(R) [G(Q, \bar{R}) + \sum_{n=1}^\infty \frac{d^n G(Q, \bar{R})}{dR^n} \frac{(R - \bar{R})^n}{n!}]. \quad (3)$$

It is worth mentioning that Eqn. (3) is applicable to general soft matter systems, provided that the shape and volume parameters, namely $P(QR)$ and $v(R)$, are known. According to the definition of probability the first central moment is always zero regardless the explicit expression of $f(R)$. In the case of spherical particles, the second order term can be expressed as

$$\frac{\sigma_R^2}{2} \frac{d^2 G}{dR^2} = v^2(\bar{R}) p^2 \left(\frac{x^2}{2} \frac{d^2}{dx^2} + 6x \frac{d}{dx} + 15 \right) P(x), \quad (4)$$

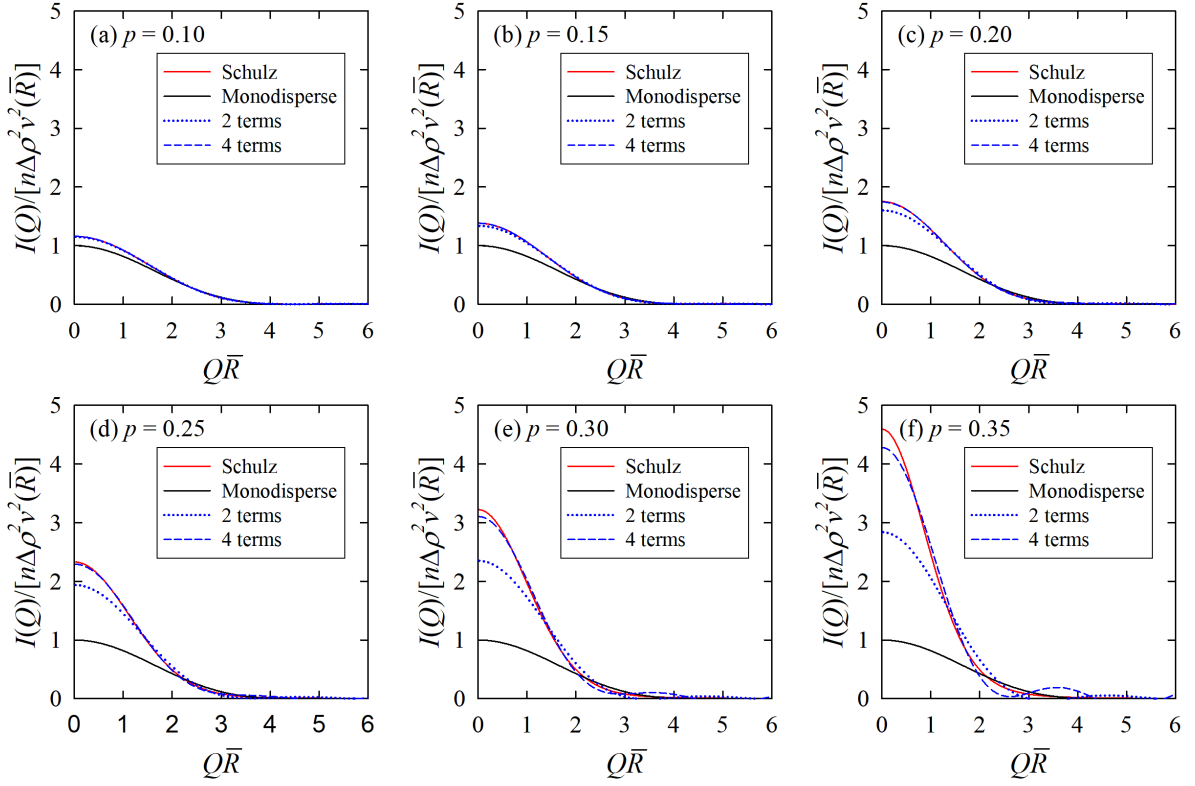


Figure 3: The decomposition of coherent scattering generated by Schulz size-distribution by central moment method up to four terms, which can be determined by the mean, variance, skewness, and kurtosis, at different degrees of polydispersity: (a) $p = 0.10$, (b) $p = 0.15$, (c) $p = 0.20$, (d) $p = 0.25$, (e) $p = 0.30$, and (f) $p = 0.35$. Red and black lines are the scattering intensities generated by Schulz size distribution and Dirac delta distribution $\delta(R - \bar{R})$.

where $x \equiv Q\bar{R}$ and $G \equiv G(Q, \bar{R})$. In the limit of $x \ll 1$, the dominant contribution comes from the third term presented in the RHS of Eqn. (4). Compared with $G(Q, \bar{R})$, the resultant correction in $I(Q)$ is around 15% of $P(Q\bar{R})$ when $p = 0.1$. The third and fourth central moments can be respectively expressed as

$$\frac{\overline{(R - \bar{R})^3}}{6} \frac{d^3 G}{dR^3} = v^2(\bar{R})p^3 \beta_1 \left(\frac{x^3}{6} \frac{d^3}{dx^3} + 3x^2 \frac{d^2}{dx^2} + 15x \frac{d}{dx} + 20 \right) P(x), \quad (5)$$

and

$$\frac{\overline{(R - \bar{R})^4}}{24} \frac{d^4 G}{dR^4} = v^2(\bar{R})p^4 \beta_2 \left(\frac{x^4}{24} \frac{d^4}{dx^4} + x^3 \frac{d^3}{dx^3} + \frac{15}{2} x^2 \frac{d^2}{dx^2} + 20x \frac{d}{dx} + 15 \right) P(x). \quad (6)$$

The third central moment vanishes for polydisperse systems characterized by symmetric SDFs such as truncated Gaussian distribution, uniform distribution, and Schulz distribution with sufficiently large \overline{R} and small σ_R^2 . Equations (5) and (6) show that $\overline{(R - \overline{R})^3}$ and $\overline{(R - \overline{R})^4}$ are of the order of σ_R^3 and σ_R^4 and thus in the low Q regime their magnitudes are proportional to the orders of p^3 and p^4 respectively. For $p = 0.1$, the corresponding corrections are approximately 2% and 0.15% respectively. Given the statistical uncertainty ($\approx 5\%$) associated with the general experimentally measured $I(Q)$, from Eqns. (5) and (6) these higher order terms are negligible when p is small. On the other hand, when p is large, the contribution from other higher order terms surely need to be incorporated in spectral analysis. Figure 3 demonstrates the validity of the CME method for reconstructing the coherent scattering intensities of hard spheres at different degrees of polydispersity. For $p \leq 0.25$ the quantitative agreement between the ground truth intensities and its CME reconstruction up to the first four central moments has been observed. However, for $p > 0.25$, the CME reconstruction starts to deviate from the ground truth. The discrepancy mainly comes from the contributions of high central moments of the size distribution function. When p is not small enough, the CME method will not converge. The criterion for the case of hard spheres can be estimated by Eqn. (4) and is $15p^2 < 1$, and this gives rise to $p < 0.258$. Figure 4 provides additional evidence of the practicality of extracting central moments across a range of polydispersity by employing CME for fitting with scattering intensities. The results demonstrate that the 1st and 2nd central moments, which correspond to the mean and variance of the particle size distribution, can be accurately reconstructed up to a polydispersity index value of $p = 0.25$. Apparently, the higher central moments can be ignored without loss of generality. Generally, the contributions of these moments are considerably smaller than those of the 1st and 2nd moments, especially when $p < 0.25$. For the regime of $0.20 < p < 0.25$, the contributions from the higher central moments start to become discernible. Nevertheless, their contributions remain insignificant in comparison to the first and second central moments.

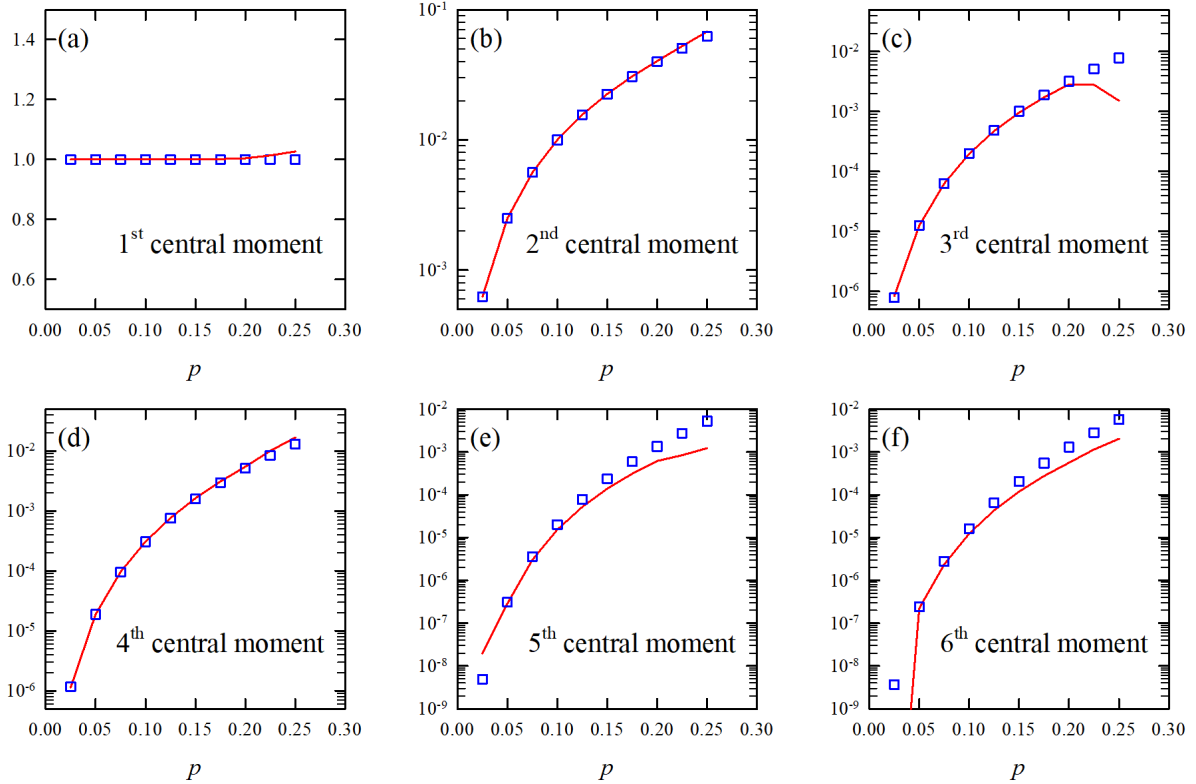


Figure 4: The six panels, (a), (b), (c), (d), (e), and (f), give the reconstruction of first six central moments by model fitting the scattering intensities using CME. The red lines are fitting results and blue squares are ground truth.

Extraction of Size Mean and Variance of Soft Balls

Having demonstrated the mathematical framework of the central moment expansion (CME) method, one can readily scrutinize the feasibility of this spectral analysis for profiling polydispersity in more general cases through numerical benchmarking: Experimentally two most commonly used parameters for quantifying polydisperse systems are \overline{R} and p . Using Eqn. (1) we first generated a series of coherent scattering intensities $I_t(Q)$ of polydisperse systems characterized by SDFs including Schulz, symmetrical beta, log-normal, uniform, and truncated Gaussian distributions with p ranging from 0.01 (nearly monodisperse systems) to 0.35 (highly polydisperse systems) and a certain \overline{R} . As demonstrated by Mittelbach and Porod⁹⁻¹¹, it is not possible to determine the size distribution and geometric shape of parti-

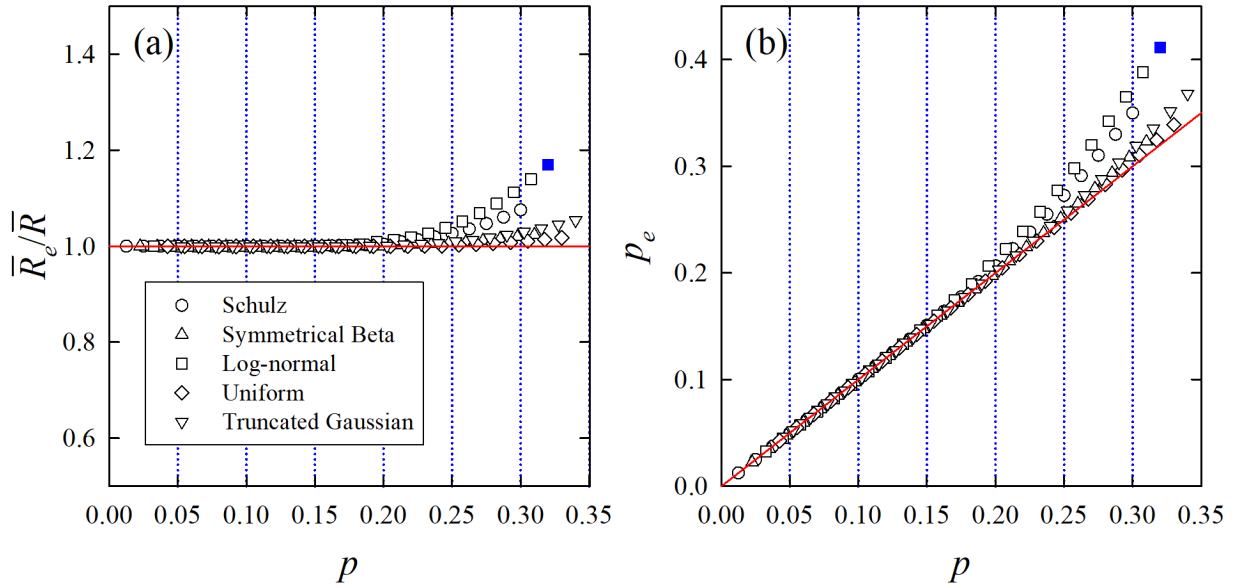


Figure 5: The comparison of extracted (a) particle mean size (R_e) and (b) polydispersity parameter p_e with the reference inputs used to generate the scattering intensities for polydisperse systems characterized by Schulz (circles), symmetrical beta (up-pointing triangles), log-normal (squares), uniform (diamonds), and truncated Gaussian (down-pointing triangles) distributions. The red lines represent the perfect agreements between the extracted values and reference inputs.

cle of a polydisperse system simultaneously in a unique manner. As a result, a pre-selected intra-particle spatial correlation function is required as an input in our approach. Here the form factor employed to produce $I_t(Q)$ deviates from that of hard sphere systems and instead uses the fuzzy ball expression $9 \exp(-x^2/50)(\sin x - x \cos x)^2/x^6$, which is commonly utilized in describing small-angle scattering behavior of globular micellar systems and soft colloids¹². Equation (3) was then used to inversely determine these two quantities of interest from $I_t(Q)$. The results given in Fig. 5 show that for systems characterized by symmetric SDFs, the extracted \bar{R} and p (marked by subscript e) show general quantitative agreements with their reference values within the entire probed range. For skewed SDFs such as Schulz and log-normal distributions, discernible deviation in estimated \bar{R} and p begins to develop when $p > 0.25$. The cause of this observation is worth exploring: First it can be straightforwardly inferred from Eqn. (4) that the CME method is valid in low Q regime when $15p^2$ is roughly

the order of one. Secondly, β_1 of symmetric SDFs is equal to zero. Numerical deviation rendered by this higher order contribution given by β_1 no longer exists in non-skewed polydisperse systems. Moreover, although in a positively skewed system population of smaller particles are favored over that of larger ones, the coherent scattering contributed by bigger particles in this asymmetric system clearly outweighs that contributed by smaller particles since the coherent scattering power of a particle is proportional to the sixth power of its size as indicated by the Rayleigh scattering law and the population distribution is based on the sampling of particle size. It is therefore not a surprise the deviation is progressively widened with an increase in p for the polydisperse systems characterized by Schulz and log-normal distributions.

To further highlight the merit of our approach, we compare it with existing nonparametric approaches. In an indirect transformation method^{6,8}, regularization and truncation in particle size are required as initial inputs for reconstructing SDFs of polydisperse systems from their coherent scattering. Implementation of this approach requires a priori knowledge of probed systems to provide unbiased interpretation of SDFs. For example, inappropriate truncation of the particle size will lead to non-negligible numerical errors in estimated σ_R^2 , p , and other higher order of central moments. There exist other commonly used approaches¹³⁻¹⁶ for inversely determining the SDFs from the coherent component of SAS in a model-free manner. However, judging from the mathematical frameworks, applicability of these methods is strictly limited for accessing the dispersity of systems consisting of particles characterized by uniform radial density profile.

Reconstruction of Size Distribution Function of Soft Balls

It is possible to reconstruct the lineshape of particle size distribution using the maximum entropy method (MEM) once the first few central moments of the distribution are provided^{17,18}. This is supported by Eqn. (3), which applies to $I(Q)$ with moderate polydispersity. As demonstration, we analyzed the $I_t(Q)$ of polydisperse fuzzy ball systems characterized by

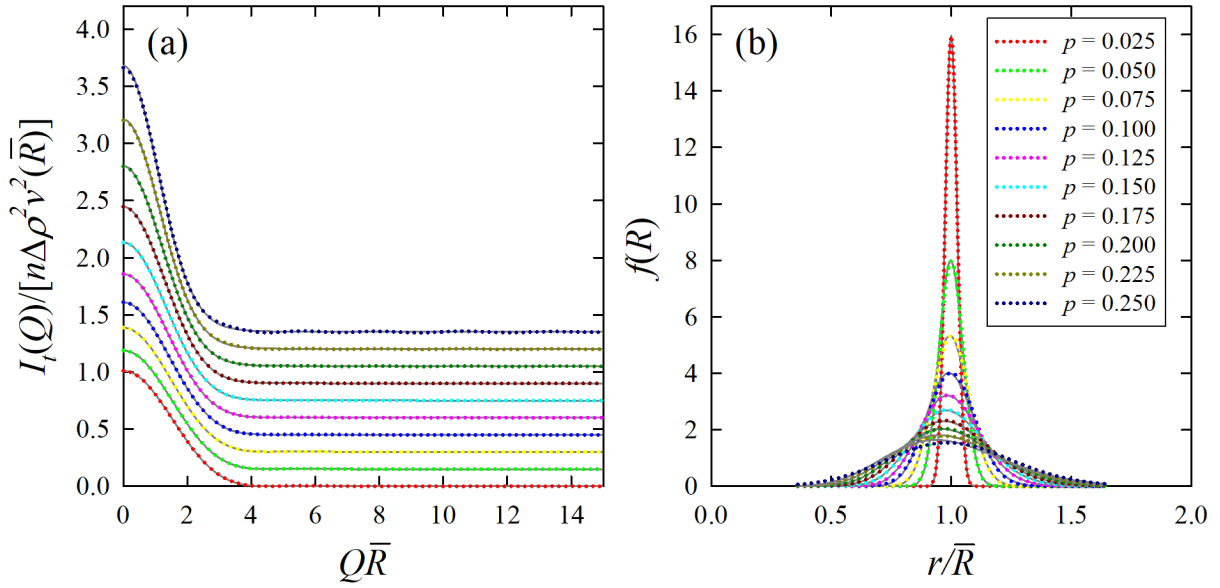


Figure 6: (a) $I_t(Q)$ of polydisperse fuzzy ball systems characterized by the Schulz distribution (solid lines) and the optimized curves via the regression analysis based on Eqn. (3) (dotted lines). Excellent quantitative agreement is observed with the probed p range. (b) The reconstructed SDF (dotted lines) and the corresponding ground truths (solid lines).

the Schulz distribution using Eqn. (3) with p ranging from 0.025 to 0.25. Figure 6(a) shows excellent agreements between $I_t(Q)$ (solid lines) and fitted curves (dotted lines). Although mathematically the complete collection of all the moments is required to determine the distribution uniquely by the MEM implementation, as demonstrated in Fig. 6(b), information from the first four central moments is sufficient to reconstruct the SDF of up to $p = 0.225$. Namely, the extracted central moments by the CME method can give reliable inputs for reconstructing SDFs by MEM. For clarity, Fig. 7 provides a more detailed comparison between the ground truth and the reconstructed distributions. In the case of $p = 0.250$ the discernible disagreement between SDFs around $r/\bar{R} = 1$ is observed because of the non-negligible contribution from higher central moments. Nevertheless, as evidenced by Figs. 4 and 5, even for the case of $p = 0.250$ the most important first two central moments related to the size mean and fluctuation can be determined accurately by the proposed CME method. In addition, it is worthwhile delving into the intriguing case of $p = 0.250$ given in Figs. 6 and 7: While discernible difference between the extracted SDF and its ground truth is observed,

the reference $I_t(Q)$ and the corresponding fitted curves appear to be indistinguishable in the length scale of Fig. 6(a). This structural ambiguity will inevitably be aggravated by the uncertainties of measured coherent intensity and the presence of incoherent scattering background which masks the coherent scattering signature in high Q region. This observation suggests the vital influence of spatial resolution on the numerical accuracy of extracted SDFs. Moreover, this statistical equivalence is not only encountered in the inversion problem of SDFs: Simple fluids characterized by radially symmetric repulsive interaction potential have been long known to be structurally identical to a hard-sphere system with an effective radius^{19–21}.

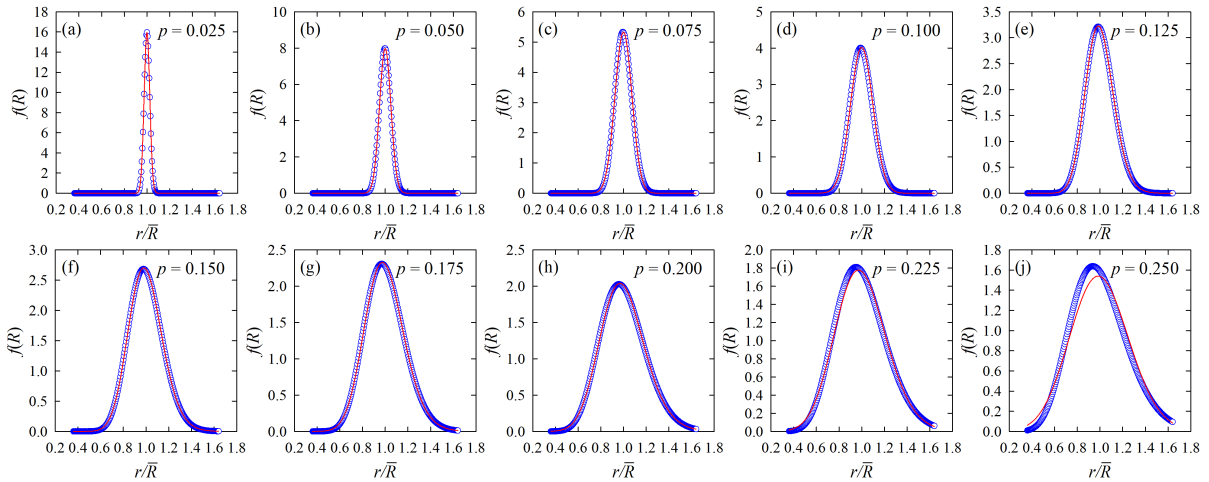


Figure 7: The comparison between the ground truth size distribution function (SDF) and the SDF reconstruction by maximum entropy method using the first four central moments obtained from Fig. 6 at different degrees of polydispersity: (a) $p = 0.025$, (b) $p = 0.050$, (c) $p = 0.075$, (d) $p = 0.100$, (e) $p = 0.125$, (f) $p = 0.150$, (g) $p = 0.175$, (h) $p = 0.200$, (i) $p = 0.225$, and (j) $p = 0.250$. In each panel, the blue circles and solid red lines are the results of ground truth and maximum entropy reconstruction.

SANS Study of L64 Micelles using CME

Lastly, we give an example of using our proposed CME approach to extract the information of polydispersity from small-angle neutron scattering (SANS) data. The selected system is the aqueous solution of Pluronic L64, a micellar system which was previously studied by

SANS^{22–28}. The surfactant weight fraction is 0.5 wt% and the solvent used in preparing the sample is D₂O. The temperature was kept at 50 °C which is above the critical micelle temperature.

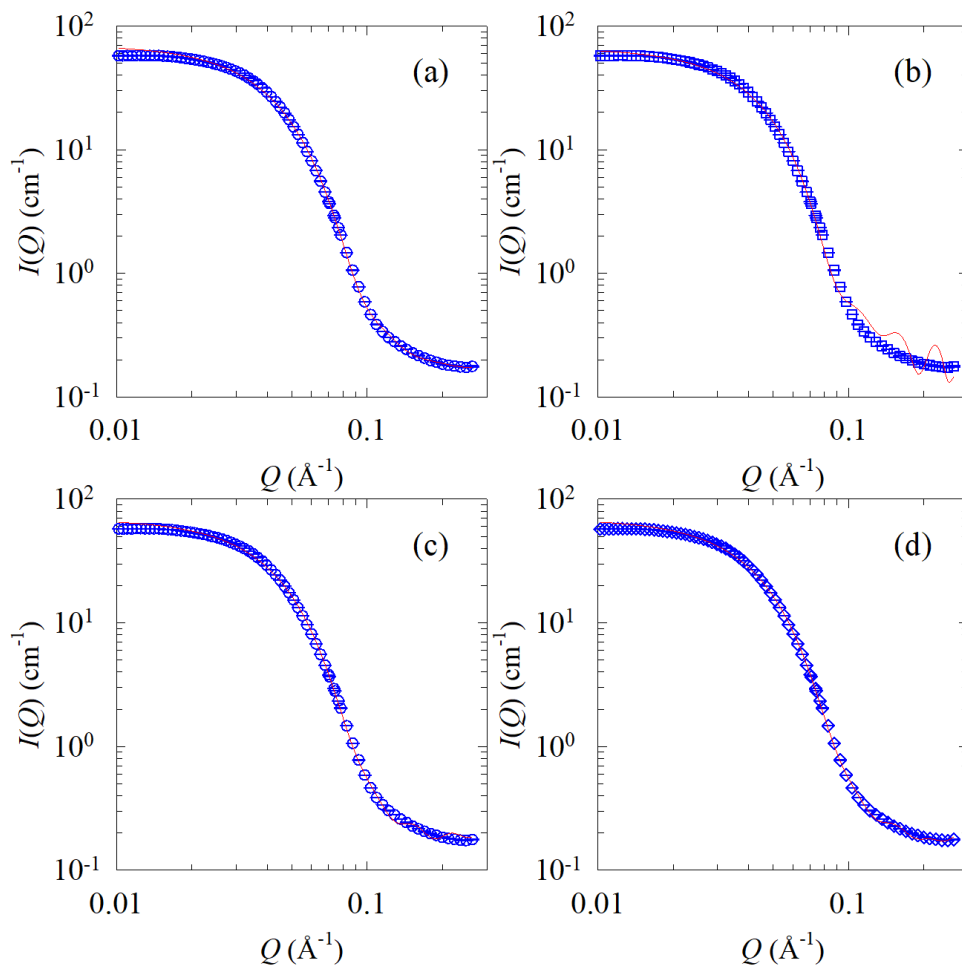


Figure 8: The SANS intensities of L64 micellar solutions and model fittings based on (a) cap-and-gown (b) core-shell (c) fuzzy spheres (d) fuzzy ellipsoid.

The SANS experiment was conducted at the EQ-SANS beamline at SNS, Oak Ridge National Laboratory; the results are shown in Fig. 8. Four different models of form factor^{24–28}, cap-and-gown (CG), core-shell (CS), fuzzy sphere (FS), and fuzzy ellipsoid (FE) respectively, which have been commonly used for describing the conformations of various globular micellar systems were used in our regression analysis of SANS data. As indicated by Fig. 8, satisfactory quantitative agreements between the experimental results (blue symbols) and

the model (red curves) are generally observed. The extracted quantitative structural information, including particle mean size and polydispersity index, is given in Table 1. Our results provide experimental support for the structural ambiguity pointed out by Mittelbach and Porod⁹⁻¹¹ that it is not possible to uniquely determine the size distribution function and particle form factor simultaneously in a model-free manner.

Table 1: The corresponding structural parameters and particle size mean and fluctuation in Fig. 8 are extracted from the SANS data fitting using the CME method with different form factor models.

Model	(Å)	(Å)	$p = \sigma_R/\bar{R}$	$(R - \bar{R})^3/\bar{R}^3$	$(R - \bar{R})^4/\bar{R}^4$
CG	Core Radius	Corona Fuzziness			
	$\bar{R} = 14.01$ (1 ± 2.6%)	27.86 (1 ± 2.5%)	0.224 (1 ± 1.3%)	0.116 (1 ± 3.6%)	0.105 (1 ± 69.0%)
CS	Core Radius	Shell Radius			
	$\bar{R} = 28.00$ (1 ± 1.3%)	45.14 (1 ± 3.3%)	0.229 (1 ± 1.3%)	0.189 (1 ± 3.7%)	0.259 (1 ± 5.1%)
FS	Radius	Radius Fuzziness			
	$\bar{R} = 39.80$ (1 ± 0.2%)	11.26 (1 ± 0.5%)	0.208 (1 ± 0.5%)	0.110 (1 ± 2.3%)	0.228 (1 ± 1.8%)
FE	Equatorial Radius	Polar Radius			
	$\bar{R} = 58.11$ (1 ± 0.3%)	34.34 (1 ± 0.8%)	0.202 (1 ± 0.2%)	0.117 (1 ± 1.2%)	0.230 (1 ± 0.8%)

Conclusion

In summary, we have developed an approach to quantify the size distribution of polydisperse systems from their coherent scattering. Via the CME method, we demonstrate that the polydispersity of systems over a wide range of size distributions can be quantitatively extracted in a model-free manner. The validity of extracting size distribution function is further benchmarked numerically. In comparison to the existing approaches, our proposed method does not require any pre-determined parametric expression of SDF as an input, and therefore provides a useful solution to fundamentally bypass the potential issue of biased data interpretation.

The present study has also indicated an area that is worth revisiting is the structural study of interacting polydisperse systems. Solving this challenging inversion problem requires addressing the inter-particle interaction and its dependence on degree of size distribution. Currently available approaches^{4,7,29–32} are unable to extract the distribution in particle size and potential parameters from the experimentally measured coherent scattering of interacting polydisperse systems in a model-free manner. Complemented by the recently developed machine learning scheme for potential inversion³³, the mathematical treatment for quantitatively characterizing heterogeneity in size and potential should remain tractable based on the extension of the expansion framework adopted in this study.

Acknowledgement

This research used resources at the Spallation Neutron Source and Center for Nanophase Materials Sciences, two DOE Office of Science User Facilities operated by the Oak Ridge National Laboratory. G.R.H. is supported by the National Science and Technology Council (NSTC) in Taiwan with Grant No. NSTC 111-2112-M-110-021-MY3. Y.W. was supported by the U.S. Department of Energy, Office of Science, Office of Basic Energy Sciences, Early Career Research Program Award KC0402010, under Contract No. DE-AC05-00OR22725. Y.S. was supported by the U.S. Department of Energy, Office of Science, Office of Basic Energy Sciences, Materials and Science and Engineering Division. The helpful discussion with Christoph U. Wildgruber is gratefully acknowledged. We gratefully appreciate the D22 SANS beamtime from ILL.

References

- (1) Tanford, C. *The Hydrophobic Effect: Formation of Micelles and Biological Membranes*, 2nd ed.; John Wiley & Sons:: New York, 1980.

- (2) Missel, P. J.; Mazer, N. A.; Benedek, G. B.; Young, C. Y. Thermodynamic Analysis of the Growth of Sodium Dodecyl Sulfate Micelles. *J. Phys. Chem.* **1980**, *84*, 1044–1057.
- (3) Moulik, S. P.; Paul, B. K. Structure, Dynamics and Transport Properties of Microemulsions. *Adv. Colloid Interface Sci.* **1998**, *78*, 99–195.
- (4) Kotlarchyk, M.; Chen, S.-H. Analysis of Small Angle Neutron Scattering Spectra from Polydisperse Interacting Colloids. *J. Chem. Phys.* **1983**, *79*, 2461–2469.
- (5) Pedersen, P., J. S. in Lindner; Zemb, T. *Neutron, X-rays and Light. Scattering Methods Applied to Soft Condensed Matter*, 1st ed.; North-Holland:: Amsterdam, 2002; Chapter 16, pp 395–397.
- (6) Glatter, O. Determination of Particle-Size Distribution Functions from Small-Angle Scattering Data by Means of the Indirect Transformation Method. *J. Appl. Cryst.* **1980**, *13*, 7–11.
- (7) Pedersen, J. S. Determination of Size Distribution from Small-Angle Scattering Data for Systems with Effective Hard-sphere Interactions. *J. Appl. Cryst.* **1994**, *27*, 595–608.
- (8) Mittelbach, R.; Glatter, O. Direct Structure Analysis of Small-Angle Scattering Data from Polydisperse Colloidal Particles. *J. Appl. Cryst.* **1998**, *31*, 600–608.
- (9) Mittelbach, P.; Porod, G. Zur Röntgenkleinwinkelstreuung kolloider Systeme – Die mittleren Durchschußlängen und die Kohärenzlänge eines kolloiden Systems; Kennzahlen zur Ermittlung von Teilchenform und Polydispersitätsgrad. *Kolloid Z. Z. Polym.* **1965**, *202*, 40–49.
- (10) Mittelbach, P. Einige spezielle Bestimmungsmethoden von Form und Polydispersität kolloider Teilchen in verdünnter Lösung mittels Röntgenkleinwinkelstreuung. *Kolloid Z. Z. Polym.* **1965**, *206*, 152–159.

- (11) Glatter, O. *Scattering Methods and Their Application in Colloid and Interface Science*, 1st ed.; Elsevier:: Amsterdam, 2018.
- (12) Huang, G.-R.; Tung, C.-H.; Chang, D.; Lam, C. N.; Do, C.; Shinohara, Y.; Chang, S.-Y.; Wang, Y.; Hong, K.; Chen, W.-R. Determining Population Densities in Bimodal Micellar Solutions Using Contrast-Variation Small Angle Neutron Scattering. *J. Chem. Phys.* **2020**, *153*, 184902, and references therein.
- (13) Riseman, J. Particle Size Distribution from Small-Angle X-ray Scattering. *Acta Cryst.* **1952**, *5*, 193–196.
- (14) Brill, O. L.; Well, C. G.; Schmidt, P. W. Determination of Particle-Diameter Distributions in Silica and Gold Suspensions. *J. Colloid Interface Sci.* **1968**, *27*, 479–492.
- (15) Vonk, C. G. On Two Methods for Determination of Particle Size Distribution Functions by Means of Small-Angle X-ray Scattering. *J. Appl. Cryst.* **1976**, *9*, 433–440.
- (16) Walter, G.; Kranold, R.; Gerber, T.; Baldrian, J.; Steinhart, M. Particle Size Distribution from Small-Angle X-ray Scattering Data. *J. Appl. Cryst.* **1985**, *18*, 205–213.
- (17) Kardar, M. *Statistical Physics of Particles*, 1st ed.; Cambridge University Press:: New York, 2007.
- (18) Huang, G.-R.; Carrillo, J. M.; Wang, Y.; Do, C.; Porcar, L.; Sumpter, B.; Chen, W.-R. An exact inversion method for extracting orientation ordering by small-angle scattering. *Phys. Chem. Chem. Phys.* **2021**, *23*, 4120–4132.
- (19) Andersen, H. C.; Weeks, J. D.; Chandler, D. Relationship between the Hard-Sphere Fluid and Fluids with Realistic Repulsive Forces. *Phys. Rev. A* **1971**, *4*, 1597–1607.
- (20) Verlet, L.; Weis, J. J. Equilibrium Theory of Simple Liquids. *Phys. Rev. A* **1971**, *4*, 939–952.

- (21) Hansen, J.-P.; McDonald, I. R. *Theory of Simple Liquids: with Applications to Soft Matter*, 4th ed.; Academic Press:: Amsterdam, 2013.
- (22) Goldmints, I.; von Gottberg, F. K.; Smith, K. A.; Hatton, T. A. Small angle neutron scattering study of PEO-PPO-PEO micelle structure in the unimer-to-micelle transition region. *Langmuir* **1997**, *13*, 3659–3664.
- (23) Goldmints, I.; Yu, G.-e.; Booth, C.; Smith, K. A.; Hatton, T. A. Structure of (deuterated PEO)-(PPO)-(deuterated PEO) block copolymer micelles as determined by small angle neutron scattering. *Langmuir* **1999**, *15*, 1651–1656.
- (24) Liu, Y.; Chen, S.-H.; Huang, J. Relationship between the microstructure and rheology of micellar solutions formed by a triblock copolymer surfactant. *Phys. Rev. E* **1996**, *54*, 1698–1708.
- (25) Svensson, B.; Olsson, U.; Alexandridis, P.; Mortensen, M. A SANS investigation of reverse (water-in-oil) micelles of amphiphilic block copolymers. *Macromolecules* **1999**, *32*, 6725–6733.
- (26) Liu, Y.; Chen, S.-H.; Huang, J. Small-angle neutron scattering analysis of the structure and interaction of triblock copolymer micelles in aqueous solution. *Macromolecules* **1998**, *31*, 2236–2244.
- (27) Yang, L.; Alexandridis, P.; Steytler, D. C.; Kositzka, M. J.; Holzwarth, J. F. Small-angle neutron scattering investigation of the temperature dependent aggregation behavior of the block copolymer Pluronic L64 in aqueous solution. *Langmuir* **2000**, *16*, 8555–8561.
- (28) Mao, G.; Sukumaran, S.; Beaucage, G.; Saboungi, M.-L.; Thiyagarajan, P. PEO-PPO-PEO block copolymer micelles in aqueous electrolyte solutions: effect of carbonate anions and temperature on the micellar structure and interaction. *Macromolecules* **2001**, *34*, 552–558.

- (29) Hayter, J. B.; Penfold, J. Determination of Micelle Structure and Charge by Neutron Small-Angle Scattering. *Colloid Polym. Sci.* **1983**, *261*, 1022–1030.
- (30) Senatore, G.; Blum, L. Size Effects and Polydispersity in Ionic Micellar Solutions within the Mean Spherical Approximation. *J. Phys. Chem.* **1985**, *89*, 2676–2682.
- (31) de Kruif, C. G.; Briels, W. J.; May, R. P.; Vrij, A. Hard-Sphere Colloidal Silica Dispersions. The Structure Factor Determined with SANS. *Langmuir* **1988**, *4*, 668–676.
- (32) D’Aguanno, B.; Klein, R. Integral-Equation Theory of Poly-disperse Yukawa Systems. *Phys. Rev. A* **1992**, *46*, 7652–7656.
- (33) Chang, M.-C.; Tung, C.-H.; Chang, S.-Y.; Carrillo, J.-M.; Wang, Y.; Sumpter, B. G.; Huang, G.-R.; Do, C.; Chen, W.-R. A Machine Learning Inversion Scheme for Determining Interaction from Scattering. *Commun. Phys.* **2022**, *5*, 46.

TOC Graphic

